Mon. Not. R. Astron. Soc. (1992) **259**, 494–504

# The power spectrum of Abell cluster correlations

J. A. Peacock[1] and M. J. West[2]
[1]*Royal Observatory, Blackford Hill, Edinburgh EH9 3HJ*
[2]*Sterrewacht Leiden, Postbus 9513, 2300 RA Leiden, The Netherlands*

Accepted 1992 May 26. Received 1992 April 2

**ABSTRACT**

We have carried out a power-spectrum analysis of the very large-scale spatial inhomogeneities in the distribution of Abell clusters. The data used consist of an all-sky sample volume-limited at redshift $z < 0.08$, containing a total of 427 clusters, for which the completeness of spectroscopic redshifts is 92 per cent for richness class $R \geq 1$ and 85 per cent for $R = 0$.

Using this sample, we have re-examined the evidence for clustering anisotropies in redshift space, to see whether the cluster selection probability is uniform on the sky. For the $R = 0$ clusters, we find a very strong anisotropy signal: there appear to be many pairs of clusters which are close on the sky, but lie at very different redshifts. However, for $R \geq 1$ clusters this effect is absent: there is no evidence that the close pairs of clusters reflect anything other than true spatial correlations. For these richer clusters, the small-scale correlation function may be described by $\xi(r) = (r/r_0)^{-\gamma}$ with $r_0 = 21.1 \pm 1.3\ h^{-1}$ Mpc and $\gamma = 2.0 \pm 0.2$. There is good evidence that the clustering strength is an increasing function of richness.

On large scales, the power-spectrum analysis detects significant inhomogeneities in the cluster distribution with wavelengths $> 100\ h^{-1}$ Mpc. However, the cluster distribution is more uniform on these scales than would be predicted from an extrapolation of the small-scale power-law clustering. Converting the results to cell-count variances, the extrapolated rms fluctuation between cubes of side $100\ h^{-1}$ Mpc is $\sigma = 0.48$, whereas $\sigma = 0.32 \pm 0.03$ is observed. Thus the distribution of Abell clusters adds further evidence to previous indications that the power spectrum of galaxy clustering has a break, with reduced power for wavelengths $\lambda \gtrsim 100\ h^{-1}$ Mpc.

**Key words:** galaxies: clustering – large-scale structure of Universe.

## 1 INTRODUCTION

In 1958, Abell published his catalogue of rich clusters of galaxies and noted that their spatial distribution seemed to be non-uniform. More than three decades later, the extent and interpretation of this inhomogeneity remains a source of cosmological controversy. The first determination of the spatial two-point correlation function for these objects (Bahcall & Soneira 1983, hereafter BS) indicated an amplified version of the galaxy correlation function: $\xi_{cc} \simeq (r/25\ h^{-1}\ \mathrm{Mpc})^{-1.8}$ (as usual, $h \equiv H_0/100$ km s$^{-1}$ Mpc$^{-1}$), with evidence of cluster correlations extending to scales of at least $r = 50\ h^{-1}$ Mpc. BS further noted a richness dependence of the correlation function, with richer clusters tending to be more strongly clustered than poorer ones. It was soon shown that rare massive objects such as Abell clusters would in general be expected to display enhanced clustering, owing to their identification as high peaks in the density field (Kaiser 1984). However, the degree of amplification found by BS has proved difficult to account for without introducing more large-scale power in the underlying density field than would be expected in the popular cold dark matter (CDM) model (e.g. Lumsden, Heavens & Peacock 1989).

As a result, the BS analysis has been subjected to quite intense scrutiny, and a number of objections have been raised by various authors. First, the size of the sample used by BS was rather small (104 clusters with measured redshifts); consequently, realistic error bars on $\xi_{cc}$ are quite large, and thus it is possible that the true clustering could in fact be considerably smaller (Ling, Frenk & Barrow 1986).

More seriously, suggestions have been made that the Abell catalogue itself is not fit for statistical analysis. Sutherland (1988) and Sutherland & Efstathiou (1991) have claimed that the selection of Abell clusters is non-uniform on the sky, with a tendency to find pairs of clusters close in projection, but at very different redshifts. On application of an algorithm designed to correct for this 'projection bias', Sutherland (1988) found that the scalelength in $\xi_{cc}$ dropped from the BS $r_0 = 25\ h^{-1}$ Mpc to $r_0 = 14\ h^{-1}$ Mpc, with no evidence of any cluster correlations beyond $50\ h^{-1}$ Mpc, and no dependence of $\xi_{cc}$ on cluster richness. Other recent developments have seemed to support this claim: the anisotropic clustering seen in the BS sample persists in the recent Huchra et al. (1990) large sample of Abell cluster redshifts, but is not seen in a set of clusters selected from the UKST/APM galaxy survey, which again show a low value of $r_0$ (Dalton et al. 1992; Efstathiou et al. 1992). However, a number of other recent studies (West & van den Bergh 1991; Bahcall & West 1992; Jing, Plionis & Valdarnini 1992; Plionis & Borgani 1993; Postman, Huchra & Geller 1992) have questioned the reality of the 'Sutherland effect', giving a variety of arguments in favour of the large correlation length and the richness dependence of $\xi_{cc}$ found by BS.

In contrast to the above studies, we were interested in using Abell clusters to probe clustering on scales much larger than $r_0$. It has recently become clear that the best statistic to use when searching for weak large-scale inhomogeneities is not $\xi$, but cell-count variance (Efstathiou et al. 1990; Saunders et al. 1991) or direct power-spectrum analysis (Peacock & Nicholson 1991, hereafter PN; Peacock 1991). In many ways, the power spectrum is a simpler and more robust quantity than the correlation function, since it measures *directly* the contribution of different scales to the observed density field, and thus can be more readily compared with theory. This is particularly true on large scales, where $\xi$ is very sensitive to assumptions about the mean density $\overline{n}$ (because $1 + \xi \propto \overline{n}^{-1}$ and $\xi \ll 1$). The power spectrum also has the advantage that it must be positive; if this criterion is violated, then there is a clear indication of problems with the data – which would be much less obvious if one considered $\xi$ alone. Thus, although in principle the power spectrum is simply the Fourier transform of the correlation function, in practice it is desirable to determine it directly from the data rather than attempting to transform the noisy estimate of $\xi_{cc}$, especially on large scales. Nevertheless, it would clearly be unwise to apply these methods to Abell clusters if the catalogue was corrupted by small-scale non-uniform selection; this prompted us to begin by re-examining the issue of anisotropic clustering.

Since the study of large-scale clustering requires the largest possible sample volume, we compiled the most complete set of redshifts we could locate for Abell clusters over the whole sky (i.e. including the southern clusters of Abell, Corwin & Olowin 1989, which have generally been neglected in the above studies). This data base and its completeness are discussed in Section 2. Section 3 derives $\xi_{cc}$ from these data and looks at the evidence for anisotropy; we shall argue that this is confined to the less rich clusters, so that power-spectrum analysis of the rich Abell cluster distribution is valid. This analysis of large-scale clustering is performed in Section 4, and the results are discussed in Section 5.

## 2 DATA

The two cluster catalogues of Abell (1958) and Abel, Corwin & Olowin (1989, hereafter ACO) contain a total of 4073 distinct clusters of richness class $R \geq 0$ ($\geq 30$ members within a projected radius of $1.5\ h^{-1}$ Mpc, to a distance-independent magnitude limit). The original design criterion was that the catalogue should be complete to redshift $z \simeq 0.2$. Redshifts are available for only a small fraction of these clusters, however; the most recent published compilations contain only 758 redshifts in the north (Struble & Rood 1991) and 115 in the south (ACO), many of which are based on only a single galaxy redshift. We have been able to improve on this somewhat, especially in the south. First, we have supplemented the above redshift compilations by including redshifts gathered from a number of more recent studies (Muriel, Nicotra & Lambas 1990, 1991; Vettolani et al. 1990; Batuski et al. 1991; Cappi et al. 1991; Postman et al. 1992). Secondly, we have received generous personal communications of unpublished cluster redshifts (principally from C. Collins). Thirdly, we have deduced some cluster redshifts via a cross-comparison with other redshift catalogues – looking for galaxies which lay within a few Abell radii in projection of a cluster centre, and whose redshifts agreed with the cluster estimated redshift (see below). This procedure is clearly well motivated when using the radio-galaxy data base of PN, where many of the galaxies are expected to be cluster members; 16 redshifts were obtained in this manner. We also used 16 redshifts obtained in a similar way by Andernach (1991, and private communication). This yielded a total of 1095 cluster redshifts [we did not include the 33 clusters listed in table 2 of Struble & Rood (1991) as having erroneous published redshifts]. We chose to work with observed heliocentric redshifts, rather than including corrections to the Local Group frame. Our list of redshifts will not be completely correct, since a significant portion of the published and unpublished cluster redshifts are based on a single galaxy. In some cases, the redshift will turn out to be that of an unrelated foreground galaxy, rather than that of the cluster. Some of these errors can be identified by considering estimated redshifts for clusters, to which we now turn.

### 2.1 Redshift estimation

As well as eliminating incorrect redshifts, we need to estimate redshifts for the remaining Abell clusters which lack spectroscopy, in order to assess the completeness of any sample we may define. The main distance indicator for Abell clusters has traditionally been $m_{10}$: the red magnitude of the tenth-brightest cluster member, which forms an approximate standard candle. It has also long been known that improved estimates may be obtained by taking into account the Scott effect: $m_{10}$ is brighter for the richer clusters. For the southern clusters, more information is available in the form of magnitudes for first- and third-ranked galaxies. We can also attempt to improve things by considering the Galactic extinction for each cluster. Abell assumed a standard slab model, but a good estimate of each individual value can now be obtained from the 100-μm Galactic emission as measured by the *IRAS* satellite (Rowan-Robinson et al. 1991): $A_V = 0.06\,(I_{100}/\mathrm{MJy\ sr^{-1}})$. Without prejudice, we may look

for a linear relation between $\log z$ and all the pieces of information available to us. Least-squares minimization yields the following estimators:

$$\log_{10} z = -4.692 + 0.207\, m_{10} - 0.214\, A_V + 0.163 \log_{10} N \quad \text{(north)}$$

$$\log_{10} z = -2.956 + 0.049\, m_1 + 0.050\, m_3 + 0.067\, m_{10} - 0.226\, A_V - 0.930 \log_{10} N + 0.285 (\log_{10} N)^2 \quad \text{(south)}, \qquad (1)$$

where $N$ is the number of galaxies counted by Abell/ACO. Note that Abell's extinction correction in the north $[A_R = 0.136 (\mathrm{cosec}\,|b| - 1)]$ has been removed, and that the southern $m_{10}$ values are as measured in the blue, not corrected to the northern red system. The second-order Scott term in the south does significantly reduce the scatter.

Erroneous redshifts were detected by iteratively removing clusters with redshifts more than $3\sigma$ from the least-squares fit. This resulted in the rejection of 31 redshifts (in all but three cases, the redshift was lower than the estimate, as expected for foreground contamination). After this trimming, the rms uncertainty in the redshift estimates was 27 per cent (north) and 18 per cent (south). Because of the greater accuracy of the southern estimates, we used the southern cluster parameters for clusters found in the north–south overlap zone. Contrary to some statements in the literature, we see no evidence that the accuracy of the northern redshift estimates deteriorates beyond $z = 0.1$.

### 2.2 Completeness limits and space densities

Armed with the best available estimate of the redshift content of the Abell/ACO catalogues, we can now consider the maximal region over which a complete sample can be defined. Consider first the redshift direction. Fig. 1 shows the relative comoving densities (assuming $\Omega = 1$, as throughout this paper) in redshift shells, contrasting the contribution of clusters with spectroscopic redshifts with two estimates of the total distribution. These are obtained either by simply adopting the best estimated values for the unknown redshifts, or by adding to these a Gaussian scatter corresponding to their known fractional precision. In principle, the latter should be the better estimate; however, it is quite likely that some bias has been introduced by virtue of those clusters for which observers have tried to obtain redshifts, but failed. Since these are not published, it is hard to be precise, but it seems likely that the numbers of low-$z$ clusters might be over-predicted by including a scatter in this way. Prudence dictates that we set a redshift limit at the point where these three estimates diverge significantly. As has been found by other workers, this seems to correspond to a redshift of about 0.08. Note that, in Fig. 1 and throughout the analysis, we have excluded the zone $z < 0.01$, since it seems likely that clusters at these redshifts will have such large angular sizes that they will be hard to select in a complete way.

Now consider the sky coverage. Fig. 2 plots all clusters with redshift (true or estimated) $z < 0.08$. The obscuring effect of the Galactic plane is obvious enough, but where does it cease to be important? Abell himself gave a (latitude-dependent) limit of $|b| \simeq 30°$–$35°$ above which the catalogue was considered to be complete. However, this was to the

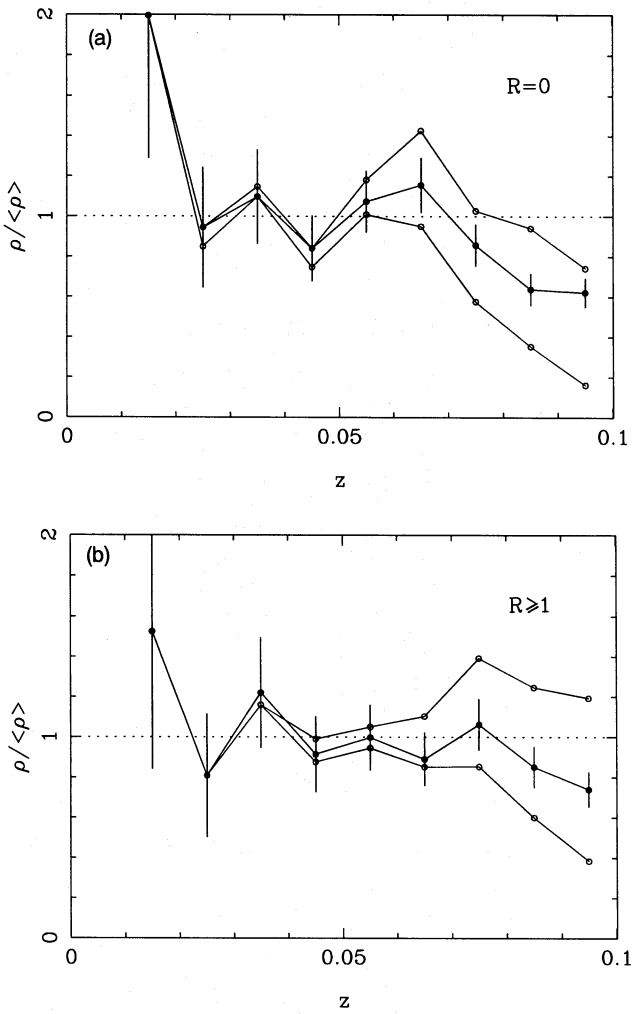


**Figure 1.** The relative comoving density of (a) $R = 0$ and (b) $R \geq 1$ clusters, assuming $\Omega = 1$. The different symbols distinguish between the use of only spectroscopic redshifts and the addition of estimated redshifts as discussed in the text. Solid points with error bars denote the data used in the analysis: measured redshifts plus estimates. The lower open circles denote measured redshifts only; the upper open circles show the effect of adding a scatter to the estimated redshifts. The uncertainties introduced by the incompleteness of spectroscopic data are unimportant for $z \lesssim 0.08$.

depth of $z \simeq 0.2$, not the much shallower limit of $z \leq 0.08$ to which we shall restrict ourselves. The clear detection of the $z \simeq 0.05$ Shapley supercluster centred at RA$\simeq 13^{\mathrm{h}}5$, Dec.$\simeq -30°$, extending down to $b \simeq 25°$ shows that one should be able to go closer to the Galactic plane. There are two advantages in doing so: the sample size increases, reducing shot noise; the selection function is more nearly isotropic, which is helpful in the power-spectrum analysis (see Section 4).

However, we need some objective guide in order to stop us going too far and inducing spurious large-scale power by including incomplete regions. For this purpose, we can use the *IRAS* extinction estimates. Fig. 3 compares the distribution of extinction values for all Abell/ACO clusters at $|b| > 20°$ with the distribution expected for a uniform coverage of that region of sky. As expected, there is a deficit of clusters at large values of extinction: the observed distribu-

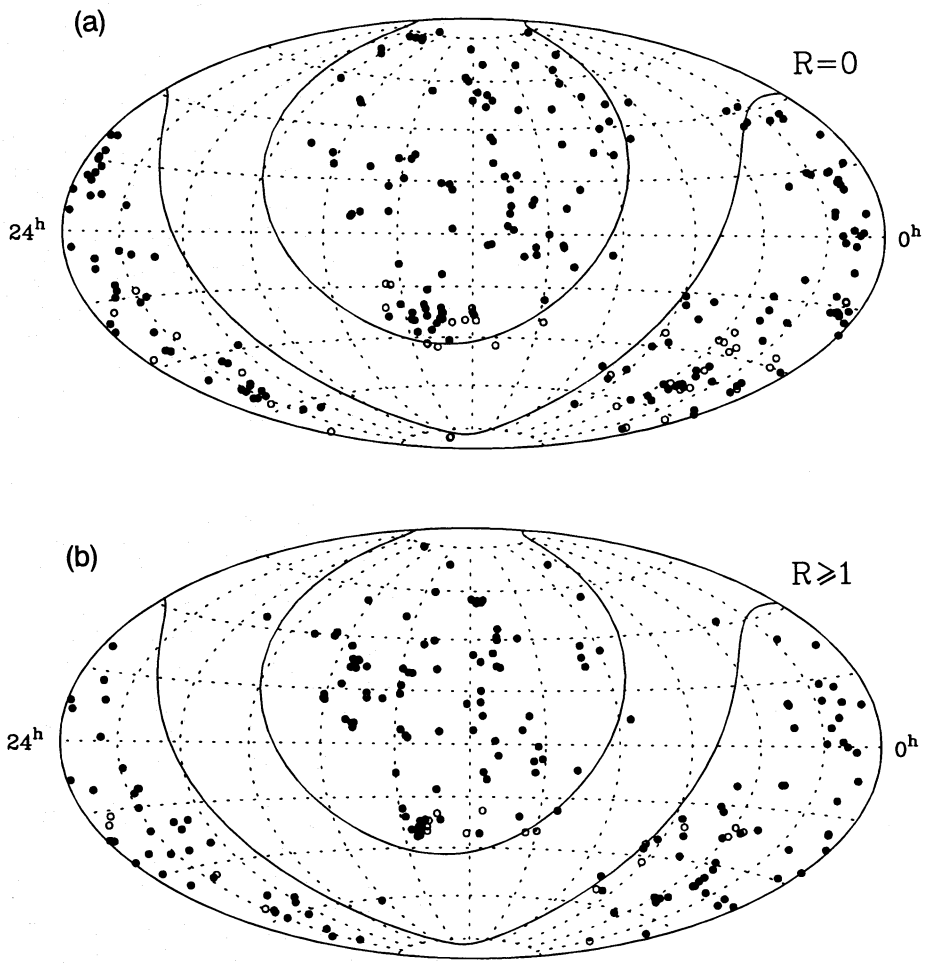


**Figure 2.** The sky distribution of (a) $R=0$ and (b) $R\geq 1$ clusters with $z<0.08$, using an Aitoff projection. Open circles denote clusters with estimated redshifts. The solid lines are loci of constant galactic latitude: $|b|=20°$.

tion virtually cuts off for $A_V>0.5$ mag. For smaller values of extinction, conversely, the two distributions are very similar in shape. Given that this is the distribution for all clusters, whereas we shall only be interested in those with $z<0.08$, it seems quite safe to adopt the limit of $A_V=0.5$ as defining the completeness of our sample. The figure of 0.5 mag is conservative: if clusters can be seen to $z>0.2$ in regions of low extinction, then they should be easily seen to $z=0.08$ in the presence of this much extinction. Fig. 4 shows a plot of the region of sky affected in this way. It would be possible to use this mask directly in any clustering analysis. However, we have preferred the approach of defining a simple region on the sky which corresponds closely to this plot. Our main criterion is

$$|b|>25°, \tag{2}$$

with the additional exclusion of two regions:

$$\text{RA}=3^h\text{–}6^h, \quad \text{Dec.}=0°\text{–}35°, \qquad \text{RA}=15^h\text{–}18^h, \quad \text{Dec.}=-30°\text{–}0°. \tag{3}$$

These criteria define an area of 6.96 sr, over which there are 179 $R\geq 1$ clusters with measured redshifts $z<0.08$, plus 16 with estimated redshifts below this limit. For $R=0$ clusters, the corresponding numbers are 198 and 34; for $R\geq 2$, the numbers fall to 42 and 3. We shall treat the estimated redshifts as real data in what follows. The samples we shall use are thus 92 per cent ($R\geq 1$) or 85 per cent ($R=0$) complete in terms of spectroscopic redshifts.

We note in passing that these figures imply comoving densities of $7.2\times10^{-6}$ $h^3$ Mpc$^{-3}$ ($R\geq 1$), $1.7\times10^{-6}$ $h^3$ Mpc$^{-3}$ ($R\geq 2$) and $8.6\times10^{-6}$ $h^3$ Mpc$^{-3}$ ($R=0$). This is slightly higher than the BS figure of $6\times10^{-6}$ $h^3$ Mpc$^{-3}$ for $R\geq 1$, but by no means as high as the $8\text{–}12\times10^{-6}$ $h^3$ Mpc$^{-3}$ suggested by Scaramella et al. (1991). The reason for this is that Scaramella et al. made a correction for incompleteness near the Galactic plane based on fitting to the *total* surface density of clusters at all redshifts. A number of authors have also followed this procedure of allowing for a Galactic latitude dependence when calculating $\xi_{cc}$. However, as discussed above, the effect of obscuration should be to reduce total numbers via the loss of more distant clusters; it thus seems incorrect to scale the densities of nearby clusters in this way.

## 3 THE CORRELATION FUNCTION AND TESTS FOR ISOTROPY

We now evaluate $\xi_{cc}$ using the above samples. We follow the standard procedure of generating random catalogues with

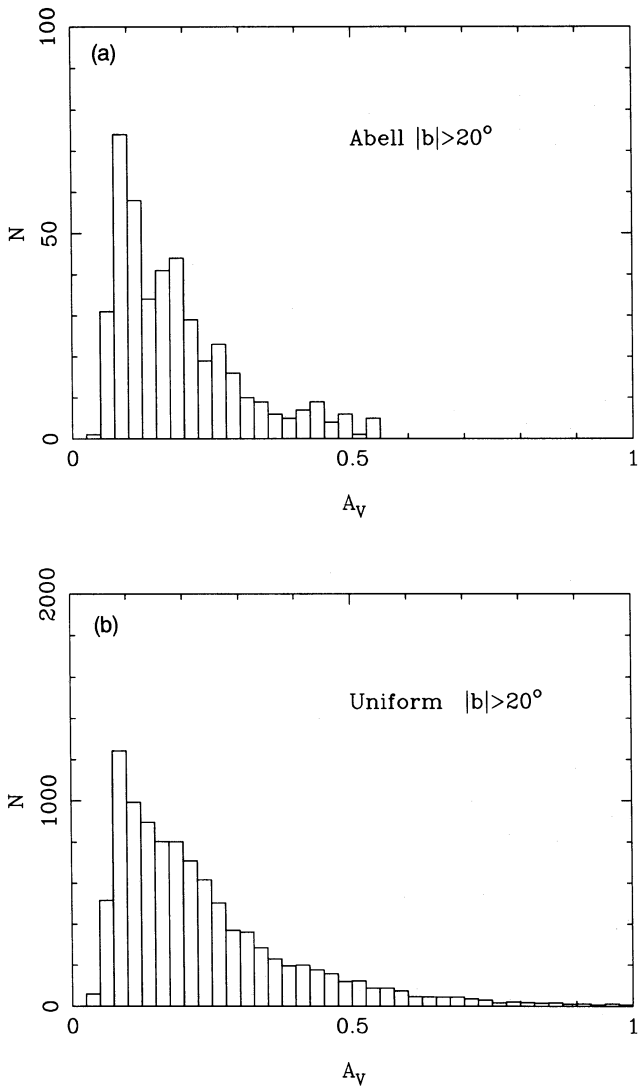


**Figure 3.** The distribution of extinction values (a) for clusters at $|b|>20°$; (b) for a uniform coverage of this part of the sky. The cluster catalogue is clearly highly incomplete for $A_V>0.5$ mag.

uniform sky coverage and redshifts drawn from the observed redshift distribution (with 1000 km $s^{-1}$ smoothing). The correlation function is estimated via the ratio of cluster–cluster pairs ($N_{cc}$) to cluster–random ($N_{cr}$) pairs:

$$1+\xi_{cc}=\frac{2N_{cc}}{N_{cr}}\frac{n_r}{n_c}, \tag{4}$$

where $n_c$ and $n_r$ are the number densities of the two catalogues and the factor 2 corrects for the fact that each distinct cluster pair is only counted once. We shall initially plot just the Poisson error bars on $\xi_{cc}$,

$$\frac{\delta\xi}{1+\xi}=\frac{1}{\sqrt{N_{cc}}}, \tag{5}$$

and will consider more realistic error estimates below.

Fig. 5 shows the resulting correlation function, divided according to richness class; strong clustering is evident. A power-law fit $\xi=(r/r_0)^{-\gamma}$ to the data for $r<50\ h^{-1}$ Mpc yields $r_0=21.1\pm1.3\ h^{-1}$ Mpc and $\gamma=2.0\pm0.2$ for $R\geq1$. The case of $R=0$ is curious in that there is strong clustering at large $r$, which flattens at small separations. The formal fit is rather flat: $r_0=20.6\pm1.5\ h^{-1}$ Mpc and $\gamma=1.5\pm0.2$; we shall consider the reasons for this below. For now, if we ignore the bins at $r<10\ h^{-1}$ Mpc and force $\gamma=2$, then $r_0=21.1\pm1.5\ h^{-1}$ Mpc. Finally, although the sample is very small, the $R\geq2$ clusters display a vast clustering amplitude; fixing $\gamma$ at 2 and using all data out to $r=100\ h^{-1}$ Mpc gives the enormous value $r_0=45\pm5\ h^{-1}$ Mpc.

Until the anisotropy analysis has been performed, one should of course not take these figures as definitive, and we shall not attempt to draw conclusions concerning the richness dependence of $\xi_{cc}$ at this stage. Nevertheless, given an estimate of $\xi_{cc}$, we can now ask whether the Poisson errors are realistic. The criterion for this to be the case is for $4\pi n_c J_3$ to be small, where $4\pi J_3$ is the volume integral of $\xi_{cc}$. For $r_0\simeq21\ h^{-1}$ Mpc, $\gamma\simeq2$ and $n_c\simeq7\times10^{-6}\ h^3$ $Mpc^{-3}$, $4\pi n_c J_3\simeq(r/26\ h^{-1}$ Mpc), so that the small-separation data (which mainly determine the parameters of any power-law fit

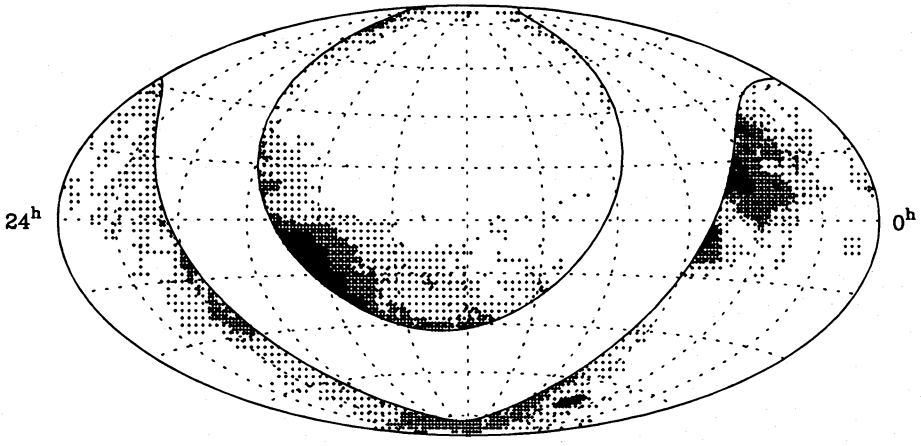


**Figure 4.** Regions of the sky at $|b|>20°$ with high extinction as estimated from *IRAS* 100-$\mu$m emission. Black indicates $A_V>1$ mag; heavy shading indicates $A_V>0.5$ mag; light shading indicates $A_V>0.25$ mag.

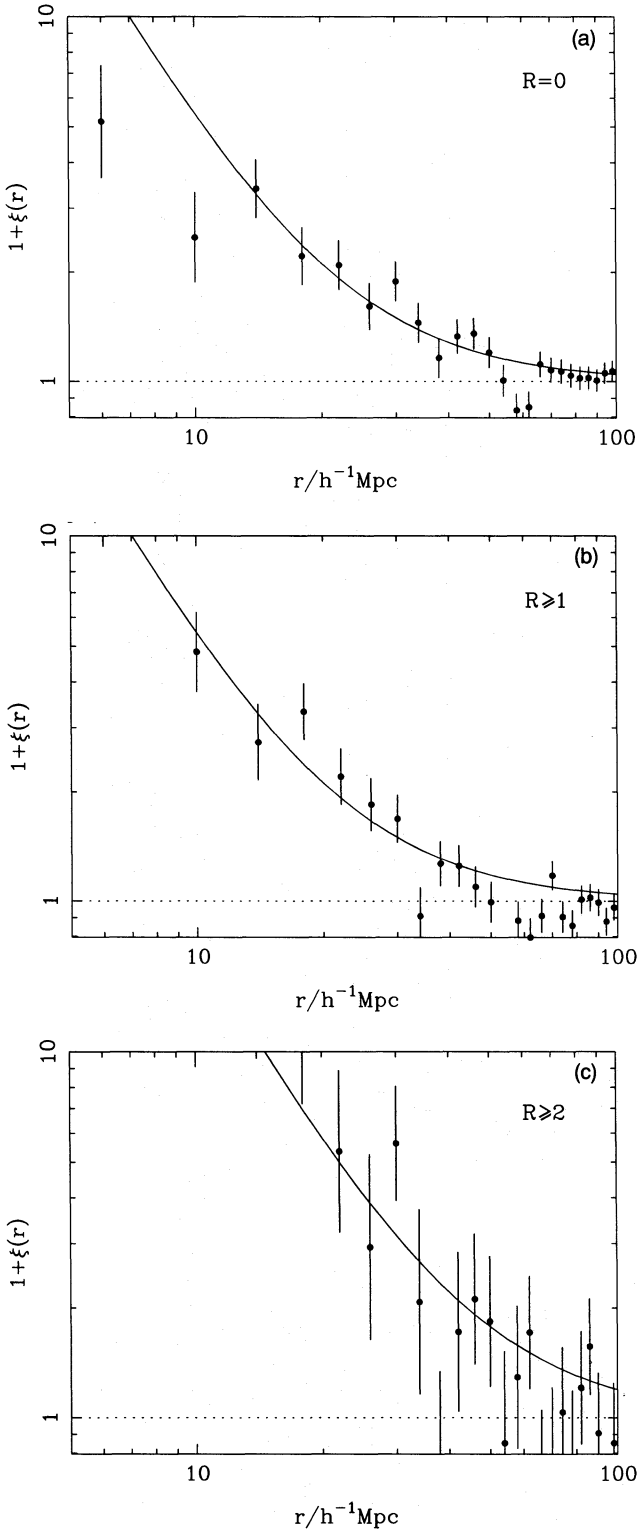


**Figure 5.** The two-point correlation function in redshift space for (a) $R=0$; (b) $R\geq 1$; and (c) $R\geq 2$ clusters. The solid lines show the model $\xi=(r/21\ h^{-1}\ \mathrm{Mpc})^{-2}$ in (a) and (b) and $\xi=(r/45\ h^{-1}\ \mathrm{Mpc})^{-2}$ in (c).

to $\xi_{cc}$) should be adequately represented by Poisson errors, at least for $R\leq 1$. For the $R\geq 2$ clusters, the signal originates at sufficiently large $r$ that the Poisson errors will be a significant underestimate. Given this and the very small sample size, one should not read too much into our $R\geq 2$ result. Furthermore, it is possible that line-of-sight superposition could be a serious problem in the very richest clusters: if the true richness distribution had a sharp cut-off, then the clusters of greatest apparent richness would all be objects with richness biased high by superposition. Any such effect will be largest in dense regions, and could in principle lead to a strong spurious spatial modulation of the distribution of the apparently richest clusters. However, the result is certainly not due to the ultra-rich Shapley concentration alone; raising the Galactic-latitude limit so as to exclude Shapley does not lower the $R\geq 2$ $\xi_{cc}$ significantly. It is therefore hard to see how $r_0$ as small as 21 $h^{-1}$ Mpc could be consistent with the data for $R\geq 2$ clusters.

We now consider in detail the issue of anisotropy. The same random catalogue procedure as above may be used to estimate $\xi_{cc}$ as a function of radial ($\pi$) and transverse ($\sigma$) separations ($\sigma$ defined as $\sqrt{r^2-\pi^2}$, where $\pi$ is taken as the difference in radii for the two objects). This yields a function $\xi(\sigma,\ \pi)$ which would be circularly symmetric for an ideal sample in the absence of redshift errors or peculiar velocities. The actual result is shown in Fig. 6, and is clearly some way from this ideal. For $R=0$ clusters, there is a tail of correlation at $\sigma=0$ beyond $\pi=100\ h^{-1}$ Mpc, which is the effect first noted by Sutherland (1988). Thus it would appear that there is indeed some corruption of the Abell catalogue by spurious line-of-sight pairs of $R=0$ clusters; the effect is far too extended to be attributed to any plausible peculiar velocity, or even to erroneous redshifts (Fig. 6 is not significantly affected by the inclusion of estimated redshifts). It seems likely that this anisotropy is responsible for the rather flat circularly averaged $\xi_{cc}$ seen in Fig. 5(a).

However, a very different picture emerges when we consider $R\geq 1$ clusters (Fig. 6b). Although there is some elongation in the redshift direction, this is of strictly limited extent: there is little evidence for clustering in the region at $\pi>50\ h^{-1}$ Mpc normally adopted by Sutherland and coworkers as a signature of spurious associations (except at very large $\pi$; this is discussed below). Fig. 7 shows cuts through the contours of Fig. 6 at varying values of $\sigma$. This illustrates well the tail of clustering out to the largest $\pi$ values ($\xi\simeq 1$ at $\sigma=0$) which applies for $R=0$ clusters, together with its absence for $R\geq 1$.

Fig. 7 also shows the results of the radial anisotropy which would be produced by peculiar velocities or redshift errors. The correlation function is convolved in the radial direction:

$$\xi(\sigma,\pi)=\int_{-\infty}^{\infty}\xi_{\mathrm{true}}(\sigma,r)\,f(\pi-r)\,\mathrm{d}r$$
$$=\frac{r_0^{\gamma}}{\sqrt{2\pi}\sigma_v}\int_{-\infty}^{\infty}[\sigma^2+(\pi-x)^2]^{-\gamma/2}\ \exp(-x^2/2\sigma_v^2)\,\mathrm{d}x, \qquad (6)$$

where the latter expression applies for power-law clustering and a Gaussian dispersion. Fig. 7 shows the model $\xi=(r/21\ h^{-1}\ \mathrm{Mpc})^{-2}$ convolved with a Gaussian of rms pairwise dispersion $\sigma_v=1000$ km s$^{-1}$. For $R\geq 1$ clusters, this provides a good fit; the high degree of clustering means that the value of $r_0$ deduced by working in redshift space is hardly different from that which applies in real space – unlike the case of ordinary galaxy clustering. This velocity dispersion (roughly 700 km s$^{-1}$ for a single cluster) is probably too high

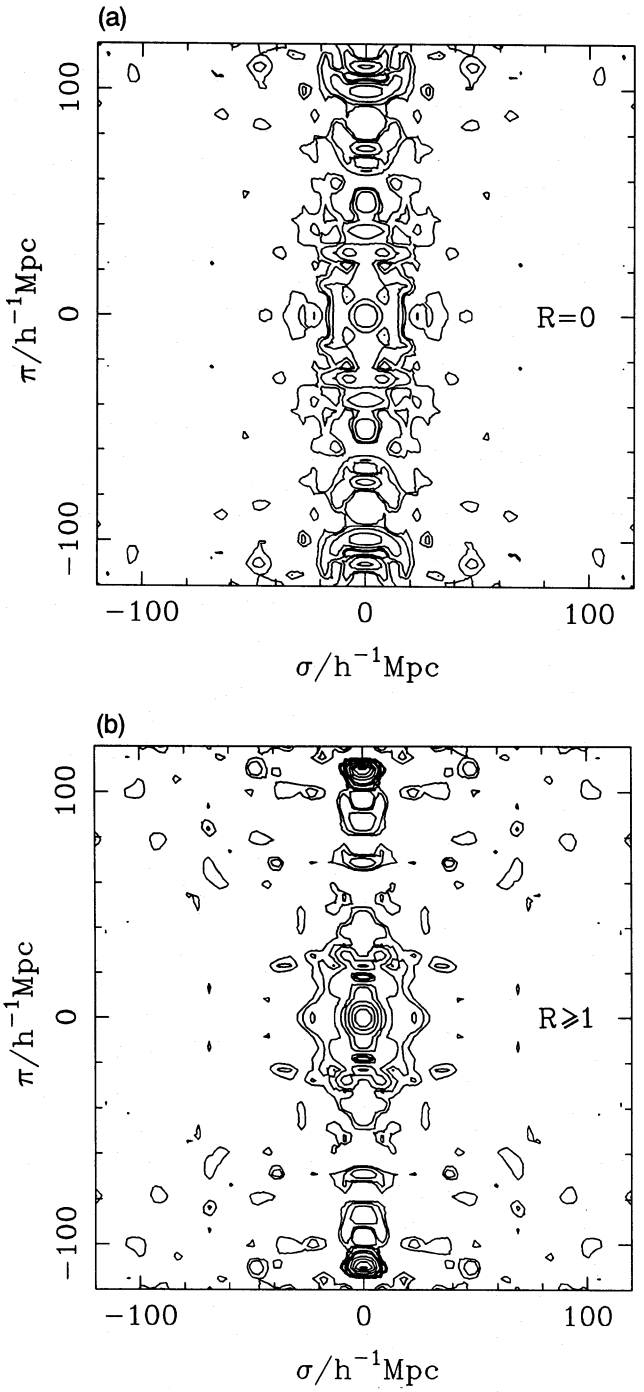


**Figure 6.** The cluster–cluster correlation function as a function of radial ($\pi$) and transverse ($\sigma$) separations. Although pair separations are by definition positive, we have continued the plot to negative values of $\pi$ and $\sigma$ by reflection, to allow the eye to judge the deviations from circular symmetry more easily. The contour values are $\xi = 0.5, 1, 2, 4, 6, 10$. Note the existence of very strong anisotropy in the case of $R = 0$ clusters and contrast this with the case of $R \geq 1$, where there is little evidence for significant clustering at $\pi > 50\ h^{-1}$ Mpc (see the text for discussion of the 'blip' at $\sigma = 0$, $\pi \simeq 120\ h^{-1}$ Mpc for $R \geq 1$).

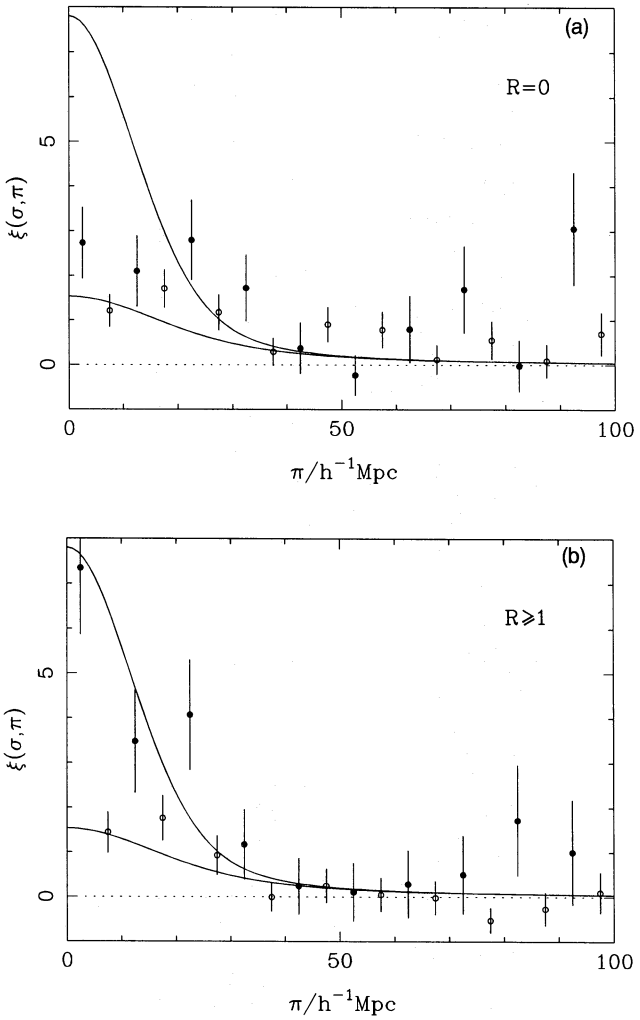


**Figure 7.** Cuts through the contours of Fig. 6 at $\sigma = 0$ (solid points) and $\sigma = 10\ h^{-1}$ Mpc (open circles) for (a) $R = 0$ and (b) $R \geq 1$ clusters. Note the tail of clustering to large $\pi$ in the former case. The solid lines show the model $\xi = (r/21\ h^{-1}\ \mathrm{Mpc})^{-2}$, allowing for a pairwise Gaussian dispersion of 1000 km s$^{-1}$ in the redshift direction.

to represent peculiar motions (Lucey & Carter 1988; although see Mould et al. 1991), but seems a perfectly reasonable figure given that many of the redshifts we have used are based on a single galaxy, plus the use of some estimated redshifts, and the undoubted presence in the data base of some undetected redshift errors.

We conclude from the above analysis that the so-called 'Sutherland effect' is real but limited. The Abell catalogue clearly has some tendency to include clusters which lie close on the sky, but which are not physically associated. However, this effect appears to be confined to the less rich clusters, and to be absent for those with richness classes $R \geq 1$. In fact, Abell clearly stated that his catalogue was only intended to be statistically useful for $R \geq 1$, and that $R = 0$ clusters were included simply as a finding list. Our results indicate that Abell achieved this aim, and bear tribute to the astonishing quality and precision of his work. It is possible to understand how it might have been thought that the richer clusters were also corrupted. Consider Fig. 6(b) again: there appears to be some strong clustering at $\sigma = 0$, $\pi = 120\ h^{-1}$ Mpc, which must be spurious on the above discussion, and which is clearly not part of any extended tail of clustering. Inspection of the data shows that this feature is entirely due to *one* cluster: A3565 at $z = 0.0119$, which lies in the foreground of

the Shapley concentration – about ten $R \geq 1$ clusters at $z \simeq 0.05$. There is thus a large contribution to the pair count at this separation. Now add the fact that the expected number of pairs at $\sigma \simeq 0$ is very small (expected pair count $\propto 2\pi\sigma\, \mathrm{d}\sigma\, \mathrm{d}\pi$), and it is easy to see how a large excursion in $\xi$ can result. It is certainly possible that A3565 is a case where the close angular proximity of other clusters in the exceptionally rich Shapley system has resulted in the spurious inclusion of one cluster, but this hardly suggests a general overcounting of close pairs. Nevertheless, in a small sample such as that of BS, such an effect could help to give the appearance of a tail of spurious associations. We also note the work of Jing et al. (1992), who have pointed out that apparent anisotropies can be generated in small samples by elongated superclusters which happen to lie along the line of sight. Taken together, these points argue that there are no grounds for using the behaviour at large $\pi$ to make a correction to the small-scale clustering properties of $R \geq 1$ clusters.

We shall not consider $R = 0$ clusters further in this paper. Although the Sutherland (1988) method could be used to obtain a corrected $\xi_{\mathrm{cc}}$, this technique is not applicable to power-spectrum analysis. Nevertheless, we emphasize that anisotropy clearly makes a large contribution to $\xi_{\mathrm{cc}}$ for $R = 0$ clusters; the true clustering length of these objects must be substantially below 21 $h^{-1}$ Mpc. If we add to this argument our very large (albeit noisy) correlations for $R \geq 2$ clusters, then our results strongly support the concept of a richness dependence of $\xi_{\mathrm{cc}}$.

## 4 POWER-SPECTRUM ANALYSIS

### 4.1 Method

Having established that the richer Abell clusters appear to be a good set of objects for statistical analysis, with a uniform number density and isotropic clustering on large scales, we now attempt to quantify their clustering via power-spectrum analysis.

For this purpose it will be assumed that the Universe is periodic within some large cubical volume, $V$. The mass density can then be expressed as the sum

$$\rho(\boldsymbol{x}) = \overline{\rho}\left[1 + \sum_{k \neq 0} \delta_{\boldsymbol{k}} \exp -i\boldsymbol{k}\cdot\boldsymbol{x}\right], \tag{7}$$

where $k$ denotes *comoving* wavenumber ($k \equiv 2\pi/\lambda$), and $\delta$ the dimensionless density contrast $\delta\rho/\rho$. If we know the Fourier coefficients $\delta_{\boldsymbol{k}}$, we can obtain the power spectrum of the density perturbation field, $P(k) \equiv |\delta_{\boldsymbol{k}}|^2$. We shall generally express the power spectrum in dimensionless form, as the variance per $\ln k$ [$\Delta^2 = \mathrm{d}\sigma^2/\mathrm{d}\ln k \propto k^3 P(k)$]:

$$\Delta^2(k) \equiv \frac{V}{(2\pi)^3}\, 4\pi k^3 P(k) = \frac{2}{\pi}\, k^3 \int_0^\infty \xi(r)\, \frac{\sin kr}{kr}\, r^2\, \mathrm{d}r. \tag{8}$$

The first definition of $\Delta^2$ uses the Fourier convention of Peebles (1980); the second is independent of convention, which is the advantage of this notation. For a pure power-law correlation function, $\xi(r) = (r/r_0)^{-\gamma}$,

$$\Delta^2(k) = \frac{2}{\pi}\,(kr_0)^{\gamma}\Gamma(2-\gamma)\sin\frac{(2-\gamma)\pi}{2}, \tag{9}$$

where $\Gamma$ is the usual gamma function. For $\gamma = 2$, equation (9) reduces to just $\Delta^2(k) = (kr_0)^2$.

As discussed in Section 1, for large scales, the power spectrum (or, equivalently, cell-count analysis) is a superior tool to $\xi(r)$. Consider the Fourier relation between $\xi$ and $\Delta^2$: $\xi = \int \Delta^2(k)(\sin kr/kr)\, \mathrm{d}k/k$. The result for $\xi$ at large separations is a mixture of modes, with a large 'leakage' of high-$k$ power because the window function $\sin kr/kr$ declines rather slowly. Since the small-scale power is often large, this can swamp any signal from low $k$. Worse, the *uncertainties* on $\xi$ are dominated by this small-scale term, so it is hard to subtract the unwanted small-scale contribution with any accuracy. Thus, although the correlation function and the power spectrum are equivalent for ideal data, it can be better in practice to measure the power spectrum directly. The truth of this proposition is readily demonstrated by Fig. 5: $\xi$ becomes quite noisy for $r \gtrsim 30\ h^{-1}$ Mpc and it is hard to tell whether any significant clustering is actually present. Nevertheless, as we shall now show, it is possible to detect genuine fluctuations in the cluster distribution with wavelengths in excess of 100 $h^{-1}$ Mpc using the power-spectrum method.

In outline, the power spectrum is estimated as follows (see PN for details). For a set of $N$ objects located at positions $\boldsymbol{x}$, one first evaluates the discrete Fourier transform:

$$\delta_{\boldsymbol{k}} = \sum N^{-1} \exp i\boldsymbol{k}\cdot\boldsymbol{x}. \tag{10}$$

In practice, one grids the data and uses a Fast Fourier Transform (FFT) thereby imposing periodic boundary conditions, so that the allowed values of $k$ are $(l^2 + m^2 + n^2)^{1/2} 2\pi/L$, where $l$, $m$, $n$ are integers and $L$ is the side of the cube. For a uniformly sampled cubical survey, these coefficients would yield directly the sum of any true clustering power and the shot noise due to discreteness of the objects:

$$\langle |\delta_{\boldsymbol{k}}|^2 \rangle = P_{\mathrm{true}} + 1/N. \tag{11}$$

Our definition of the discrete transform means that $|\delta_{\boldsymbol{k}}|^2$ is the contribution to the fractional density variance from one mode: $\Delta^2(k)$ could thus be deduced by subtracting the shot noise from $|\delta_{\boldsymbol{k}}|^2$ and adding the resulting $P_{\mathrm{true}}$ values for the modes in a given shell in $k$-space.

In practice, we do have to contend with observational selection, which produces a varying background density: $n_{\mathrm{b}} = f(\boldsymbol{x})\overline{n}$. The corrections this introduces are as follows.

(1) The Fourier coefficients obtained are proportional to the transform of $f(\boldsymbol{x})[1 + \delta(\boldsymbol{x})]$, so the transform of $f$ needs to be subtracted, which may be done by analysing a random catalogue as above.

(2) In the absence of phase correlations between clustering pattern and mask (fair sample hypothesis), we end up with just a convolution of power spectra:

$$P_{\mathrm{obs}} = P_{\mathrm{true}} * |f_k|^2. \tag{12}$$

(3) Apart from smoothing the power spectrum, this convolution also changes the normalization, as may be seen by considering the case of a uniform cubical survey of volume $V$ embedded in a larger cube of volume $V'$. Using the density of states for the larger volume to count modes causes a multiple counting of modes, and therefore causes

$P(k)$ to be too high by a factor $V'/V$. We must therefore apply the correction

$$P(k) \rightarrow P(k) \frac{(\int f \mathrm{d}^3x)^2}{\int f^2 \mathrm{d}^3x \int \mathrm{d}^3x}. \quad (13)$$

For the present case, if we embed the data set in a cube just large enough to contain a sphere of radius $z = 0.08$ (453 $h^{-1}$ Mpc on a side), this correction factor is 3.45.

After this correction, we can now sum $P$ values over a $k$-space shell and convert to $\Delta^2(k)$ by dividing by the thickness of the shell in $\ln k$. Minimal Poisson error bars (which are a good approximation at large wavelength; see PN) are obtained by counting the number of modes in the shell ($m$), scaling $m$ by the above factor to correct for multiple counting ($m' = m/3.45$ here), and using

$$\delta(\Delta^2) = \frac{\sqrt{2m'}}{N} \Big/ \Delta \ln k. \quad (14)$$

The factor 2 arises becauses only half the modes are independent owing to the reality of the density field, i.e. $\delta_k(\boldsymbol{k}) = \delta_k^*(-\boldsymbol{k})$.

### 4.2 Results

Fig. 8(a) shows the power-spectrum results for $R \geq 1$ clusters. Included on the plot for comparison is the power-law spectrum which is the transform of the best-fitting small-scale correlation function from Section 3 [$\xi = (r/21\ h^{-1}$ Mpc$)^{-2}$]. There are several features worthy of note. First, the amplitude of the high-$k$ power is well described by the power-law fit, confirming the equivalence of this procedure to $\xi(r)$ as a means of describing the small-scale clustering. Secondly, power is detected out to wavelengths well in excess of 100 $h^{-1}$ Mpc. Although there have been previous suggestions of such very large-scale structure in the Abell cluster distribution (e.g. Tully 1986, 1987), this is the first time that such inhomogeneities have been properly quantified. It is worth emphasizing that it would be very hard to distinguish between this power spectrum and one which was truncated at $\lambda = 100\ h^{-1}$ Mpc, using only the correlation function of Section 3. Last, and most interestingly, there is clear curvature in the power spectrum, with the largest wavelength points falling well below a power-law extrapolation of the small-scale clustering.

This is illustrated in Fig. 8(b), where we compare the shape of the Abell power spectrum with other galaxy clustering data. This is an updated version of Fig. 2 from Peacock (1991), with the addition of the Abell data, scaled down by a factor of 9 to match the small-scale clustering. The overall curvature of the power spectrum is reasonably well described by the fitting formula advocated by Peacock (1991) as a good fit to the galaxy data from the APM survey (Maddox et al. 1990):

$$\Delta^2(k) = \frac{0.039\, y^4}{1 + y^{2.4}}; \qquad y \equiv k/0.025\ h\,\mathrm{Mpc}^{-1}. \quad (15)$$

The large-scale break in this function therefore now receives independent support from both the radio galaxy and Abell cluster distributions. As discussed by Efstathiou, Sutherland & Maddox (1990) and by Peacock (1991), this power spectrum only agrees in shape with the linear-theory spectrum in an adiabatic CDM model when the density is low: $\Omega h \simeq 0.2$.

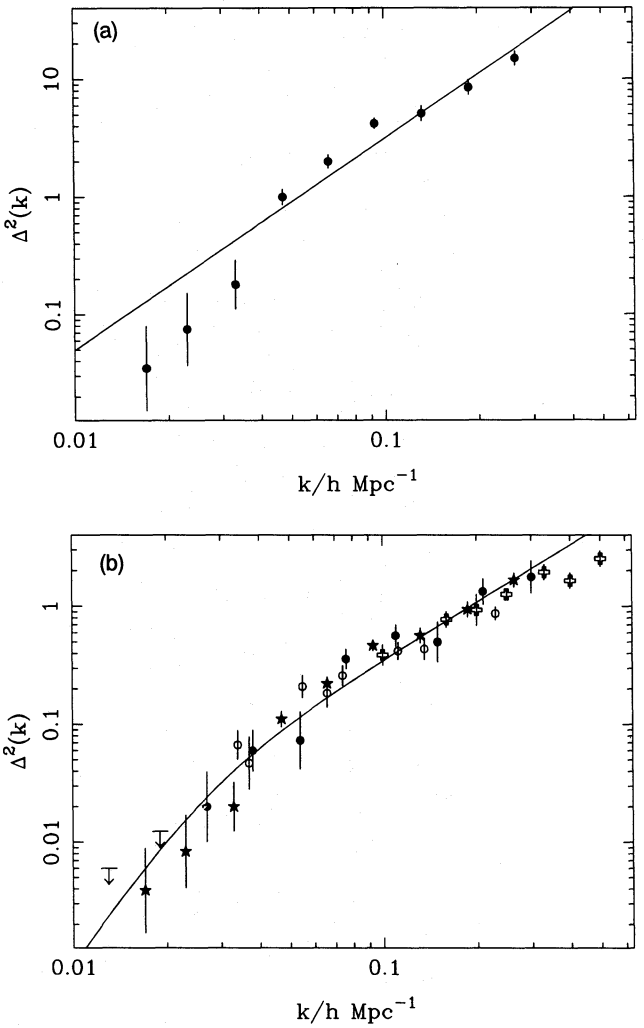


**Figure 8.** (a) The $R \geq 1$ Abell power-spectrum results, plotted as the fractional density variance per ln(wavenumber) against comoving wavenumber ($k = 2\pi/\lambda$). The solid line is the transform of the correlation function shown in Fig. 5: $\Delta^2(k) = (kr_0)^2$ with $r_0 = 21$ $h^{-1}$ Mpc. (b) The Abell results of Fig. 8(a) included on the composite power spectrum plot of Peacock (1991); this has a vertical normalization scaled to describe the redshift-space clustering of *IRAS* galaxies. The stars show the Abell cluster data, divided by a factor 9. The solid line is the fitting formula described in the text. The other symbols are radio galaxies divided by a factor 3 (solid points plus upper limits); *IRAS* (open circles); *CfA* (open crosses). The overall agreement on the shape of the clustering power spectrum is remarkably good.

One important question is whether the break in the Abell power spectrum could be artifical, caused by normalization effects. Because the global mean density of clusters is unknown and had to be estimated from the sample to hand, one clearly tends to underestimate the power in any modes whose wavelengths approach the size of the sample. PN showed that this effect is approximately given by

$$\Delta^2(k) \rightarrow (1 - |f_k|^2)\Delta^2(k), \quad (16)$$

where $|f_k|^2$ is the power spectrum of the selection function, which is unity for $k=0$ by definition. Our conclusions are thus unaffected by normalization effects, provided we restrict attention to wavenumbers for which $|f_k|^2 \lesssim 0.1$. To see where this criterion is satisfied, we plot in Fig. 9 $|f_k|^2$ for a variety of model selection functions: uniform spheres out to radius $R$, with a variety of Galactic latitude cuts. For complete sky coverage, we have the usual formula

$$|f_k|^2 = \frac{9}{(kR)^6}(\sin kR - kR\cos kR)^2, \tag{17}$$

and so $|f_k|^2 = 0.1 \Rightarrow k = 3.1/R$. For larger zones of avoidance $|f_k|^2$ rises at large $k$, but important sidelobes do not arise unless gross limits such as $|b| \gtrsim 40°$ are imposed. For our case of $|b| > 25°$ the effects are quite unimportant. We therefore conclude that the critical wavenumber in our case of limiting redshift 0.08 is $k = 3.1/226 = 0.014$. Thus the break in the power spectrum is *not* the result of normalization effects. Furthermore, we have been able to dispense with the observed redshift distribution in this calculation, making the assumption that, for $R \geq 1$, the comoving density is uniform out to $z = 0.08$. We therefore do not need to draw from the observed redshifts to generate a random catalogue, which might in principle lead to some underestimate of large-scale clustering. In fact, PN argued that any such effect would be negligible for all-sky samples; this is certainly what we find: the result is the same whichever method of random-catalogue generation is adopted. In addition, the result is robust with respect to small variations in the sample definition (alterations of limiting redshift and sky coverage).

### 4.3 Cell-count variances

An alternative method of investigating very large-scale clustering is to smooth the distribution of objects under study with some filter, and look at how the fractional density variance ($\sigma^2$) depends on filtering scale. Methods for estimating these variances are discussed by Efstathiou et al. (1990) and Saunders et al. (1991). An alternative way of proceeding, which can be implemented very easily in the context of the present analysis, is to work in Fourier space, since the required variances are just integrals over the power spectrum times some window function, $W_k$:

$$\sigma^2 = \int_0^\infty \Delta^2(k)\, W_k^2 \frac{\mathrm{d}k}{k}. \tag{18}$$

Each grid point in $k$-space has an associated power estimate plus uncertainty (see equation 14); we can thus estimate directly cell-count variances and uncertainties thereon via a direct sum over the power in $k$-space produced from the FFT analysis.

Table 1 gives the results of this procedure for the two cells commonly discussed: Gaussian spheres of radius $R_G[W \propto \exp(-r^2/2R_G^2) \Rightarrow W_k = \exp(-k^2R_G^2/2)]$ and cubical cells of side $\ell$. The table also gives the variance expected on the pure power-law model $\xi = (r/21\ h^{-1}\ \mathrm{Mpc})^{-2}$. There is one subtlety here: for cubical cells and this power spectrum, the variance formally diverges logarithmically at high $k$. We have therefore evaluated the cell variances in both cases by summation over the same $64^3$ grid used in the data analysis, incorporating the additional $k$-space smoothing caused by binning the data. For Gaussian filtering, this alters the variances by typically only 5–10 per cent from the ideal result. The results of this process make the same point as the power spectrum: for the largest cells, the signal seen lies below an extrapolation from small scales.

## 5 DISCUSSION

We have investigated the spatial correlations of Abell clusters, using the largest available samples for which we can be confident of the completeness. We find that, provided attention is restricted to the richer clusters (which were the only ones intended by Abell to be statistically useful), there is no evidence that the catalogue selection was other than uniform on the sky, at least for $z < 0.08$ and $|b| \gtrsim 25°$. The

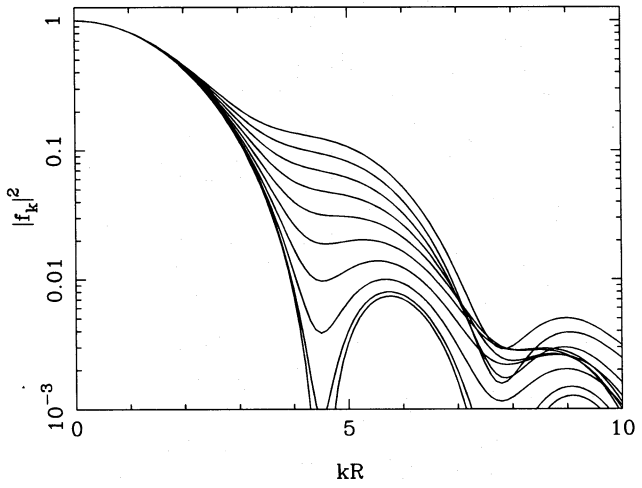


**Figure 9.** The power spectrum of window functions generated by taking a uniform ball of radius $R$ and excising Galactic latitude cuts between 0° and 45°. The sidelobes only extend the point at which $|f_k|^2 = 0.1$ significantly for latitude cuts above about 35°.

**Table 1.** Cell variances for Abell $R \geq 1$ clusters.

| $\ell_{\mathrm{cell}}/h^{-1}\mathrm{Mpc}$ | $\sigma^2_{\mathrm{obs}}$ | $\sigma^2_{\mathrm{power-law}}$ |
|---|---|---|
| 20 | $4.413 \pm 0.229$ | 5.330 |
| 30 | $2.268 \pm 0.125$ | 2.537 |
| 50 | $0.799 \pm 0.058$ | 0.943 |
| 70 | $0.320 \pm 0.035$ | 0.479 |
| 100 | $0.103 \pm 0.020$ | 0.227 |
| 150 | $0.028 \pm 0.011$ | 0.091 |
| $R_G/h^{-1}\mathrm{Mpc}$ | $\sigma^2_{\mathrm{obs}}$ | $\sigma^2_{\mathrm{power-law}}$ |
| 5 | $6.139 \pm 0.300$ | 7.514 |
| 10 | $1.861 \pm 0.106$ | 2.097 |
| 20 | $0.382 \pm 0.038$ | 0.527 |
| 30 | $0.107 \pm 0.020$ | 0.225 |
| 40 | $0.040 \pm 0.013$ | 0.119 |
| 50 | $0.019 \pm 0.009$ | 0.070 |

$\sigma^2_{\mathrm{power\text{-}law}}$: predictions assuming $\xi = (r/21\ h^{-1}\ \mathrm{Mpc})^{-2}$.

$R \geq 1$ Abell clusters appear to us to be almost entirely free from the projection contamination effects which have been the subject of so much debate in recent years.

We therefore believe that previous indications of a scale-length of $r_0 \simeq 20\ h^{-1}$ Mpc for $R \geq 1$ clusters were accurate. Furthermore, there is good evidence for a richness dependence of clustering within the Abell catalogue, with $R \geq 2$ clusters displaying enhanced correlations, and the apparent clustering of $R = 0$ clusters being artificially boosted via anisotropy effects. This is well consistent with the weak clustering found for the less rich APM clusters of Dalton et al. (1992) – see Bahcall & West (1992). We do not feel compelled to debate the source of the evident corruption of the $R = 0$ clusters. Whether the effect is psychological or could be quantified as a result of overlapping counting areas seems immaterial; the effect is sufficiently large that any attempt to correct for it, either empirically (as in Sutherland 1988) or a priori (as in Dekel et al. 1989), would yield a result in which it would be difficult to invest much faith. Our defence of the Abell catalogue should not be taken too far, however, since it is certainly the case that some Abell systems are the result of a few smaller clumps superimposed along the line of sight (e.g. A1736, Dressler & Shectman 1988; A1775, Zabludoff, Huchra & Geller 1990). Nevertheless, from the clustering point of view, these effects should be unimportant provided they result simply in a rather large scatter between true and inferred richness which is independent between different clusters. Clustering results should not be affected provided line-of-sight corruption has no large-scale correlation. A critical test of this assertion will be provided by the *ROSAT* cluster sample, but we believe that the prospects for the correctness of the Abell result are good.

Using power-spectrum analysis, we have shown that the distribution of Abell clusters is more uniform on large scales than would be predicted by an extrapolation of the power-law clustering seen on small scales, although the power-law model is a good description of the clustering to quite large scales, $\lambda \simeq 100\ h^{-1}$ Mpc. We note that a very similar result has been obtained independently by Einasto, Gramann & Tago (1993). The shape of the power spectrum for Abell clusters would appear to be consistent with that for galaxies, scaled up by a factor 9 in comparison with galaxy clustering in redshift space. This sort of amplification can quite plausibly be accounted for via the Kaiser (1984) mechanism. There are thus grounds for believing that the spatial correlations of Abell clusters fit into a consistent picture of large-scale structure. The question of whether the cluster data are consistent with a specific model such as CDM is then equivalent to asking whether the model can account for the power spectrum of galaxy clustering. Conversely, any model which can account convincingly for the large-scale power seen in the galaxy distribution should stand a good chance of also accounting for the correlations of Abell clusters.

## ACKNOWLEDGMENTS

We thank C. Collins for generous communication of unpublished redshift data. MJW is supported by the Netherlands Foundation for Research in Astronomy (NFRA).

## REFERENCES

Abell G. O., 1958, ApJS, 3, 211
Abell G. O., Corwin H. G, Olowin R. P., 1989, ApJS, 70, 1 (ACO)
Andernach H., 1991, in Latham D., da Costa L., eds, Workshop on Large-Scale Structures and Peculiar Motions. Astron. Soc. Pacif. Conf. Series 15, p. 279
Bahcall N. A., Soneira R. M., 1983, ApJ, 270, 20 (BS)
Bahcall N. A., West M. J., 1992, ApJ, 392, 419
Batuski D. J., Burns J. O., Newberry M. V., Hill J. M., Deeg H. J., Laubscher B. R., Elston R. J., 1991, AJ, 101, 1983
Capi A., Focardi P., Gregorini L., Vettolani G., 1991, A&AS, 88, 349
Dalton G. B., Efstathiou G., Maddox S. J., Sutherland W. J., 1992, ApJ, 390, L1
Dekel A., Blumenthal G. R., Primak J. P., Olivier S., 1989, ApJ, 338, L5
Dressler A., Shectman S. A., 1988, AJ, 95, 296
Efstathiou G., Sutherland W., Maddox S. J., 1990, Nat, 348, 705
Efstathiou G., Kaiser N., Saunders W., Lawrence A., Rowan-Robinson M., Ellis R. S., Frenk C. S., 1990, MNRAS, 247, 10P
Efstathiou G., Dalton G. B., Sutherland W., Maddox S. J., 1992, MNRAS, 257, 125
Einasto J., Gramann M., Tago E., 1993, MNRAS, in press
Huchra J. P., Henry J. P., Postman M., Geller M., 1990, ApJ, 365, 66
Jing Y.-P., Plionis M., Valdarnini R., 1992, ApJ, 389, 499
Kaiser N., 1984, ApJ, 284, L9
Ling E. N., Frenk C. S., Barrow J. D., 1986, MNRAS, 223, 21P
Lucey J. R., Carter D., 1988, MNRAS, 235, 1177
Lumsden S. L., Heavens A. F., Peacock J. A., 1989, MNRAS, 238, 293
Maddox S. J., Efstathiou G., Sutherland W. J., Loveday J., 1990, MNRAS, 242, 43P
Mould J. R., Staveley-Smith L., Schommer R. A., Bothun G. D., Hall P. J., Han M. S., Huchra J.. P., Roth J., Walsh W., Wright A. E., 1991, ApJ, 383, 467
Muriel H., Nicotra M., Lambas D. G., 1990, AJ, 100, 339
Muriel H., Nicotra M., Lambas D. G., 1991, AJ, 101, 1997
Peacock J. A., 1991, MNRAS, 253, 1P
Peacock J. A., Nicholson D., 1991, MNRAS, 253, 307 (PN)
Peebles P. J. E., 1980, The Large-Scale Structure of the Universe. Princeton Univ. Press, Princeton, NJ
Plionis M., Borgani S., 1993, MNRAS, in press
Postman M., Huchra J. P., Geller M. J., 1992, ApJ, 384, 404
Rowan-Robinson M., Hughes J., Jones M., Leech K., Vedi K., Walker D. W., 1991, MNRAS, 249, 729
Saunders W., Frenk C., Rowan-Robinson M., Efstathiou G., Lawrence A., Kaiser N., Ellis R., Crawford J., Xia X.-Y., Parry I., 1991, Nat, 349, 32
Scaramella R., Zamorani G., Vettolani G., Chincarini G., 1991, AJ, 101, 342
Struble M. F., Rood H. J., 1991, ApJS, 77, 363
Sutherland W. J., 1988, MNRAS, 234, 159
Sutherland W. J., Efstathiou G., 1991, MNRAS, 248, 159
Tully R. B., 1986, ApJ, 303, 25
Tully R. B., 1987, ApJ, 323, 1
Vettolani G., Chincarini G., Scaramella R., Zamorani G., 1990, AJ, 99, 1709
West M. J., van den Bergh S., 1991, ApJ, 373, 1
Zabludoff A. I., Huchra J. P., Geller M. J., 1990, ApJS, 74, 1